

Implementation of the Divergence-Free and Pressure-Oscillation-Free Projection Method for Solving the Incompressible Navier-Stokes Equations on the Collocated Grids

Yu-Xin Ren^{1,*}, Miao'er Liu² and Hanxin Zhang³

¹ Department of Engineering Mechanics, Tsinghua University, Beijing 100084, China.

² CNOOC Research Center, Beijing 100027, China.

³ National Key Laboratory for CFD, Beijing 100083, China.

Received 14 June 2006; Accepted (in revised version) 23 November 2006

Available online 22 January 2007

Abstract. In this paper, a divergence-free and pressure-oscillation-free projection method for solving the incompressible Navier-Stokes equations on the non-staggered grid is presented. The exact discrete projection method is used to compute the velocity field, which ensures the discrete divergence of the velocity field is zero. In order to eliminate the odd-even decoupling in the pressure field, a filtering procedure is proposed and applied to the pressure field. We have shown this filter recovers the grid scale ellipticity in the pressure field and the odd-even decoupling can be removed effectively. The proposed numerical scheme is further verified through numerical experiments.

AMS subject classifications: 65M06, 76D05, 65M15

Key words: Incompressible Navier-Stokes equations, projection methods, non-staggered grids, pressure filtering.

1 Introduction

Conventional numerical methods for solving the incompressible Navier-Stokes (N-S) equations in terms of the primitive variables are mainly applied on the marker-and-cell (MAC) [13] type staggered grids. For this type of grids, the pressure, density and other scalars are stored in the mesh cell center, the velocities are stored at the mesh cell faces and the momentum equations are solved by constructing separate control volumes around them. This arrangement makes the stencil for the pressure gradient terms in the

*Corresponding author. *Email addresses:* ryx@tsinghua.edu.cn (Y. X. Ren), liume@cnooc.com.cn (M. Liu)

momentum equations very compact. The continuity equation can be also computed directly requiring no interpolations. These two features make the staggered grid approach capable of capturing all resolvable modes and thereby preventing the odd-even decoupling or the "checkerboard" modes of the pressure field.

However, the use of the staggered grids adds geometrical complexity by the introduction of multiple control volumes. Furthermore, the staggered grid schemes become very awkward when generalizing to curvilinear meshes and unstructured grids that are commonly used to handle the complex geometries. The use of staggered grids for complex geometries leads to either high memory requirements, or inefficient solution methods or complicated equations with additional source terms [27].

An alternative form of the control volume and fluid variable positioning technique, namely the non-staggered or collocated grid arrangement, stores all the variables at the same physical location and employs only one set of control volumes. This approach reduces the geometrical complexity and shortens the long computational time needed in the conventional staggered methods and is becoming increasingly popular in practical applications.

A significant shortcoming of the non-staggered grid approach is the so called odd-even coupling phenomenon or the occurrence of "checkerboard" modes in the pressure field. When the NS equations are solved by the projection methods [5-8,14-20,23,25], this phenomenon has also been observed [22].

There are two types of projection methods, namely the "exact" discrete projection methods and the approximate projection methods [1]. In the exact projection method, the discrete Poisson equation is defined as the product of the discrete divergence operator and the discrete pressure gradient operator, and the discrete divergence of velocity is zero, or more precisely, small quantity within the convergence tolerance of the solution of the discrete Poisson equation. When second-order central difference approximations are implemented for both operators, the discrete Poisson equation corresponds to a non-compact sparse stencil and produces an oscillatory pressure field [22].

If the discrete Poisson equation is derived through a straightforward discretization of the continuous Laplacian operator, the resulting projection scheme is called the approximate projection method [1]. In this case, the discrete divergence of velocity is not zero, but is rather a function of the truncation error. For the pressure-free projection methods, the approximate projection procedure can effectively remove the checkerboard modes in the pressure field [27]. However, for the incremental-pressure projection method, it is generally not sufficient to eliminate the pressure oscillations [16]. Therefore, other supplementary measurements must be used. These measurements include the momentum interpolation technique [21] and its variants [3,4,9], various filters designed by Lai [16] and Riders [22], and the fourth-order "compact equivalent" approximation of the discrete Poisson equation [10].

Although the approximate projection methods perform well in many practical applications, they inevitably produce velocity fields that are not divergence-free in the discrete sense. The non-divergence-free velocity fields sometimes have adverse effects on the ac-

curacy of the numerical solutions [22]. In this paper, a procedure for the implementation of the second order incremental-pressure projection scheme on collocated grids is presented. In this approach, the exact discrete projection method is used to compute the velocity field, which ensures the discrete divergence-free property. In order to eliminate the odd-even decoupling in the pressure field, a filtering procedure is proposed and applied to the pressure field. Using the theory proposed in [3,24], we have shown this filter recovers the grid scale ellipticity in the pressure field and the odd-even decoupling can be removed effectively. It should be noted that the emphasis of this paper is not to study the projection method itself, but rather to design the solution procedure of the projection method on the non-staggered grid so that the numerical solution is divergence-free and pressure-oscillation-free.

This paper is organized as follows. In Section 2, we review the second-order incremental pressure projection method proposed by Brown et al. [7] for completeness. The pressure filtering technique is presented in Section 3. The ellipticity of the present method is discussed in Section 4. Sections 5 and 6 present the numerical results and the conclusions, respectively.

2 The second order projection method

The unsteady incompressible N-S equations in primitive variable form are written as

$$\frac{\partial \mathbf{u}}{\partial t} + \nabla \cdot (\mathbf{u} \otimes \mathbf{u}) + \nabla p = \nu \nabla^2 \mathbf{u} + \mathbf{f}, \quad (2.1)$$

$$\nabla \cdot \mathbf{u} = 0, \quad (2.2)$$

where \mathbf{u} , p , ν and \mathbf{f} are the velocity vector, pressure, kinematic viscosity of the fluid, and body force, respectively. We notice that the density is already absorbed in the pressure term and is not shown in Eq. (2.1). The initial conditions are

$$\mathbf{u}(\mathbf{x}, 0) = \mathbf{u}_0,$$

and the boundary conditions are

$$\mathbf{u}_b = \mathbf{w}.$$

In this paper, we only consider the two-dimensional finite volume scheme for solving the N-S equations on uniform rectangular cells for simplicity, though it is straightforward to extend the numerical scheme to three-dimensional and general control volume cases. A collocated cell arrangement is used, in which all flow variables are stored at the center of a cell or control volume.

Eqs. (2.1) and (2.2) are discretized using a second-order incremental-pressure projection method. This method is similar to that proposed by Brown et al. [7] except that the exact discrete projection is adopted. The projection method is a predictor-corrector

scheme. In the predictor step, an intermediate velocity is computed according to the discrete equations

$$\frac{(\mathbf{u}^*)_{ij}^{n+1} - \mathbf{u}_{ij}^n}{\Delta t} + D(\mathbf{u} \otimes \mathbf{u})_{ij}^{n+1/2} + Gq_{ij}^{n+1/2} = \frac{v}{2} L_h[(\mathbf{u}_{ij}^*)^{n+1} + \mathbf{u}_{ij}^n] + \mathbf{f}_{ij}^{n+1/2}, \quad (2.3)$$

where $q^{n+1/2}$ is an estimation of the pressure at time level $n+1/2$ which is taken as $q^{n+1/2} = p^{n-1/2}$, Δt is the time step, and D , G and L are the discrete divergence, gradient and Laplacian operators respectively. These operators are defined as:

$$D(*)_{ij} = D_x[\mathbf{i} \cdot (*)] + D_y[\mathbf{j} \cdot (*)], \quad (2.4)$$

$$D_x(\bullet) = \frac{(\bullet)_{i+1,j} - (\bullet)_{i-1,j}}{2\Delta x}, \quad D_y(\bullet) = \frac{(\bullet)_{i,j+1} - (\bullet)_{i,j-1}}{2\Delta y}, \quad (2.5)$$

$$G(\bullet)_{ij} = \frac{(\bullet)_{i+1,j} - (\bullet)_{i-1,j}}{2\Delta x} \mathbf{i} + \frac{(\bullet)_{i,j+1} - (\bullet)_{i,j-1}}{2\Delta y} \mathbf{j}, \quad (2.6)$$

$$L_h(\bullet)_{ij} = \frac{(\bullet)_{i+1,j} - 2(\bullet)_{ij} + (\bullet)_{i-1,j}}{\Delta x^2} + \frac{(\bullet)_{i,j+1} - 2(\bullet)_{ij} + (\bullet)_{i,j-1}}{\Delta y^2}, \quad (2.7)$$

where $(*)$ is a vector or a tensor and (\bullet) is a scalar or a vector. The \mathbf{i} and \mathbf{j} are unit basis vectors in x and y directions, respectively. To ensure the temporal second-order accuracy, the convection term is treated with the Adams-Barshforth method,

$$D(\mathbf{u} \otimes \mathbf{u})_{ij}^{n+1/2} = 1.5D(\mathbf{u} \otimes \mathbf{u})_{ij}^n - 0.5D(\mathbf{u} \otimes \mathbf{u})_{ij}^{n-1};$$

and the time derivative and the diffusion term have been discretized using the Crank-Nicholson scheme.

To solve Eq. (2.3) numerically, a certain "artificial" boundary condition must be used. According to Brown et. al [7], this boundary condition is chosen as

$$\mathbf{u}_b^* = \mathbf{w}. \quad (2.8)$$

In the corrector step, the intermediate velocity $(\mathbf{u}^*)^{n+1}$ is decomposed into a solenoidal vector \mathbf{u}^{n+1} and a curl-free vector expressed as the gradient of a potential, $\nabla \phi^{n+1}$, according to the Helmholtz-Hodge theorem. In discrete form, it can be written as

$$(\mathbf{u}^*)_{ij}^{n+1} = \mathbf{u}_{ij}^{n+1} + \Delta t G \phi_{ij}^{n+1}, \quad (2.9)$$

$$D\mathbf{u}_{ij}^{n+1} = 0. \quad (2.10)$$

Using Eqs. (2.9) and (2.10), we have

$$L_2 \phi_{ij}^{n+1} = \frac{1}{\Delta t} D(\mathbf{u}^*)_{ij}^{n+1}, \quad (2.11)$$

where $L_{2h} = DG$. It is easy to derive that

$$L_{2h}\phi_{i,j}^{n+1} = \frac{\phi_{i+2,j}^{n+1} - 2\phi_{i,j}^{n+1} + \phi_{i-2,j}^{n+1}}{4\Delta x^2} + \frac{\phi_{i,j+2}^{n+1} - 2\phi_{i,j}^{n+1} + \phi_{i,j-2}^{n+1}}{4\Delta y^2}. \quad (2.12)$$

The boundary condition of Eq. (2.11) is

$$\frac{\partial \phi_b^{n+1}}{\partial n} = 0, \quad (2.13)$$

where $\frac{\partial}{\partial n}$ stands for the normal derivative. Eqs. (2.9)-(2.13) are called the exact discrete projection because we require Eq. (2.10) to be satisfied exactly.

When ϕ^{n+1} is available after solving Eqs. (2.11) and (2.13), the velocity \mathbf{u}^{n+1} is corrected by using Eq. (2.9). The pressure can be updated according to [11]

$$p_{i,j}^{n+1/2} = q_{i,j}^{n+1/2} + \phi_{i,j}^{n+1} - 0.5v\Delta t L_h \phi_{i,j}^{n+1}. \quad (2.14)$$

Eq. (2.14) is called the consistent or rotational form pressure updating formulation. Its advantage over the traditional pressure updating method

$$p_{i,j}^{n+1/2} = q_{i,j}^{n+1/2} + \phi_{i,j}^{n+1}$$

has been discussed in [7].

3 The pressure filtering technique

The non-compact stencils of the discrete operator L_{2h} make Eq. (2.11) lack of grid level coupling. The non-physical oscillations in the pressure field can be therefore produced. It has been observed that although the distribution of ϕ and p is highly oscillatory, the fields $G\phi_{i,j}$, $L_{2h}\phi_{i,j}$ and $Gp_{i,j}$, $L_{2h}p_{i,j}$ are generally smooth. The reasons for this phenomenon are quite simple: in Eq. (2.11), the coupling is achieved on every other grid point and the operators G and L_{2h} cannot sense the grid level oscillations of the potential and pressure field. In order to achieve the grid level coupling and prevent the occurrence of the oscillations, we propose to use the filtering procedure

$$L_h(\bar{\bullet}) = L_{2h}(\bullet) \quad (3.1)$$

to smooth out the nonphysical oscillations, where (\bullet) stands for the unfiltered field, and $(\bar{\bullet})$ stands for the corresponding field after smoothing. L_h is the standard discrete Laplacian operator with compact five-point stencils defined in Eq. (2.7). This procedure is second-order accurate since

$$L_h(\bullet) - L_{2h}(\bullet) = \mathcal{O}(h^2),$$

where $h = \max(\Delta x, \Delta y)$. Therefore, the smoothing procedure will not affect the second-order accuracy of the projection scheme.

The solution procedures presented in Section 2 must be slightly modified to accommodate the filtering algorithm. Firstly, the estimated pressure is now

$$q^{n+1/2} = \bar{p}^{n-1/2}, \quad (3.2)$$

where \bar{p} is the filtered pressure. Secondly, the pressure is updated by

$$\tilde{p}_{i,j}^{n+1/2} = \bar{p}_{i,j}^{n-1/2} + \phi_{i,j}^{n+1} - 0.5v\Delta t L_h \phi_{i,j}^{n+1}, \quad (3.3)$$

and is smoothed by

$$L_h(\tilde{p}_{i,j}^{n+1/2}) = L_{2h}(\tilde{p}_{i,j}^{n+1/2}). \quad (3.4)$$

We note in the present approach, the quantity being filtered is the pressure instead of the potential ϕ ; therefore, the velocity correction procedure, Eq. (2.9), is not affected by the pressure filtering and the discrete divergence of the corrected velocity field remains to be zero as in the ordinary exact discrete projection methods.

It is apparent that in the present approach, two discrete Poisson equations must be solved in the projection procedure. Therefore, the present approach is computationally more expensive than the approximate projection methods. It should be pointed out that for some approximate projection methods, the solutions of two Poisson equations are also required with one Poisson equation being similar to Eq. (2.11) and another one being the result of the MAC projection procedure [22]. The MAC projection procedure is adopted to ensure the balance of the volumetric flux across a control volume. Because the present method is divergence-free, the MAC projection procedure is not needed in the present approach. In this paper, the Poisson equations, Eq. (2.11) and Eq. (3.4), are both solved using the GMESR algorithm presented in [26].

4 The regularity (ellipticity) of the pressure filtering procedure

As shown in [24], a scheme solving the incompressible N-S equations must be regular elliptic in order that the solution is smooth. In the present section, the regularity of the present method will be discussed. For simplicity, we neglect the advection and forcing terms in the N-S equations and consider the corresponding Stokes equations only.

We apply the discrete Laplace and the Fourier transform in time and spatial directions respectively to the proposed projection method. Denoting the transform of (\bullet) as $(\hat{\bullet})$, we have

$$(\bullet)_{i,j}^n = (\hat{\bullet}) e^{st_n + \zeta(k_x x_i + k_y y_j)}, \quad (4.1)$$

where $\zeta = \sqrt{-1}$. Applying Eq. (4.1) to Eqs. (2.3), (2.11), (2.9), (3.3) and (3.4) (neglecting

the advection and forcing terms), we obtain

$$\left[\frac{1}{\Delta t} - \frac{v\widehat{L}_h}{2} \right] \widehat{u}^* e^{s\Delta t} - \left(\frac{1}{\Delta t} - \frac{v\widehat{L}_h}{2} \right) \widehat{u} + \widehat{D}_x \widehat{p} e^{-s\Delta t/2} = 0, \tag{4.2}$$

$$\left[\frac{1}{\Delta t} - \frac{v\widehat{L}_h}{2} \right] \widehat{v}^* e^{s\Delta t} - \left(\frac{1}{\Delta t} - \frac{v\widehat{L}_h}{2} \right) \widehat{v} + \widehat{D}_y \widehat{p} e^{-s\Delta t/2} = 0, \tag{4.3}$$

$$\widehat{L}_{2h} \widehat{\phi} = \frac{1}{\Delta t} \left[\widehat{D}_x \widehat{u}^* + \widehat{D}_y \widehat{v}^* \right], \tag{4.4}$$

$$\widehat{u} = \widehat{u}^* - \Delta t \widehat{D}_x \widehat{\phi}, \quad \widehat{v} = \widehat{v}^* - \Delta t \widehat{D}_y \widehat{\phi}, \tag{4.5}$$

$$\widehat{p} e^{s\Delta t/2} = \widehat{p} e^{s\Delta t/2} + (1 - 0.5v\Delta t \widehat{L}_h) \widehat{\phi} e^{s\Delta t}, \quad \widehat{L}_h \widehat{p} = \widehat{L}_{2h} \widehat{p}, \tag{4.6}$$

where “ $\widehat{}$ ” over an operator denotes the symbol of this operator in wave number space. Eliminating \widehat{u}^* , \widehat{v}^* , $\widehat{\phi}$, \widehat{p} and \widehat{p} from Eqs. (4.2)-(4.6), we reach the following system of equations:

$$\begin{bmatrix} \widehat{A} & 0 & \widehat{D}_x \widehat{P} \\ 0 & \widehat{A} & \widehat{D}_y \widehat{P} \\ \widehat{D}_x & \widehat{D}_y & 0 \end{bmatrix} \begin{bmatrix} \widehat{u} \\ \widehat{v} \\ \widehat{p} \end{bmatrix} = 0, \tag{4.7}$$

where

$$\widehat{A} = \left(\frac{1}{\Delta t} - \frac{v\widehat{L}_h}{2} \right) e^{s\Delta t} - \left(\frac{1}{\Delta t} + \frac{\widehat{L}_h}{2} \right), \quad \widehat{P} = \frac{\widehat{L}_h e^{s\Delta t/2}}{\widehat{L}_{2h}}.$$

The determinant of Eq. (4.7) is

$$Det = -\widehat{A} e^{s\Delta t/2} \widehat{B}, \tag{4.8}$$

where

$$\widehat{B} = (\widehat{D}_x \widehat{D}_x + \widehat{D}_y \widehat{D}_y) \frac{\widehat{L}_h}{\widehat{L}_{2h}}.$$

It is apparent that the operator \widehat{B} stands for the velocity-pressure coupling effect, therefore \widehat{B} is considered only in the ellipticity analysis [2,3,24]. If \widehat{B} has no real zeros for all realizable wave number components ($0 < k_x \Delta x \leq \pi$, $0 < k_y \Delta y \leq \pi$), then the system is regular elliptic.

Armfield [2] used the h -ellipticity measure E_h of \widehat{B} to measure its degree of ellipticity, which is defined by

$$E_h = \min_{0 < k_x \Delta x, k_y \Delta y, k'_x \Delta x, k'_y \Delta y \leq \pi} \frac{\widehat{L}_h(k_x \Delta x, k_y \Delta y)}{\widehat{L}_h(k'_x \Delta x, k'_y \Delta y)} \left| \frac{\widehat{B}(k'_x \Delta x, k'_y \Delta y)}{\widehat{B}(k_x \Delta x, k_y \Delta y)} \right|.$$

According to this definition, we have $0 \leq E_h \leq 1$. When $E_h = 0$, the \widehat{B} or the corresponding numerical procedure is not elliptic; when $E_h > 0.7$, \widehat{B} is called strong elliptic. Armfield pointed out that the h -ellipticity measure E_h has a strong relation with the smoothness of the pressure field. For the projection method on staggered grid, $E_h = 1$ and the pressure

field is always smooth; for the unfiltered exact projection method on the non-staggered grid, $E_h = 0$ and the odd-even decoupling in the pressure field will be observed.

We remark that in [18], the h -ellipticity measures of the pressure-free approximate projection method [27] and the incremental-pressure approximate projection method supplemented with the momentum interpolation technique [21] or the technique proposed by Armfield [3] have been computed. It is shown that the h -ellipticity measures of these schemes are all functions of Re_G , where

$$Re_G = \frac{h^2}{\Delta t \nu}$$

and $h = \Delta x = \Delta y$ is the mesh size. For most range of Re_G , $E_h < 0.7$, and E_h will become very small as Re_G increases to a large value. Therefore, these methods are only weak elliptic for large Re_G and small oscillations in the pressure fields may still occur in such a case.

For the present method, it is easy to show that $(\widehat{D}_x \widehat{D}_x + \widehat{D}_y \widehat{D}_y) = \widehat{L}_{2h}$. Therefore,

$$\widehat{B} = \widehat{L}_h,$$

and the h -ellipticity measure of the present scheme is $E_h = 1$, which means that the present method has the same property of ellipticity with the projection method on a staggered grid and therefore the odd-even decoupling in the pressure field can be removed effectively.

5 Numerical tests

Case 1. The forced flow problem. In this test case [7], the fluid flows in a channel with periodic boundary conditions in the x -direction. A no-slip condition is prescribed at $y=0$, while a nontrivial slip condition is specified at $y=1$. The N-S equations are augmented with a forcing term in order that the solution is

$$\begin{aligned} u &= \cos(2\pi(x - \omega(t)))(3y^2 - y), \\ v &= 2\pi \sin(2\pi(x - \omega(t)))y^2(y - 1), \\ p &= -\frac{\dot{\omega}(t)}{2\pi} \sin(2\pi(x - \omega(t)))(\sin(2\pi y) - 2\pi y + \pi) \\ &\quad + v \cos(2\pi(x - \omega(t)))(\sin(2\pi y) + 2\pi y + \pi), \end{aligned}$$

where $\omega(t) = 1 + \sin(2\pi t^2)$, and the viscosity is set to $\nu = 1$. In the numerical simulation, the ratio $\Delta t/h$ is set to be 0.5. We apply the present projection scheme on a series of $N \times N$ grids with N equal to 32, 64, 128, 256, and 512, respectively. The errors of the computed velocity and pressure in both the 2- and ∞ -norm at $t=1$ are reported in Fig. 1 as functions of Δt in double logarithm scale. The second-order convergence rate is observed in both norms. Therefore, the introduction of the pressure filtering procedure does not affect the

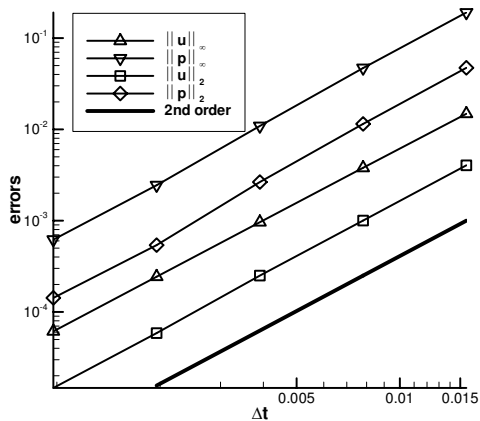


Figure 1: Errors in the pressure and u -component of velocity at $t=1$ computed using the present projection scheme for Case 1.

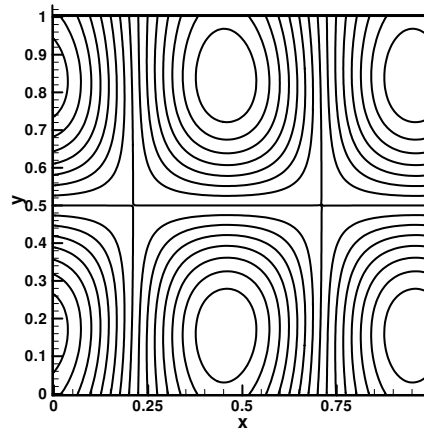


Figure 2: The pressure contours for Case 1 at $t=1$.

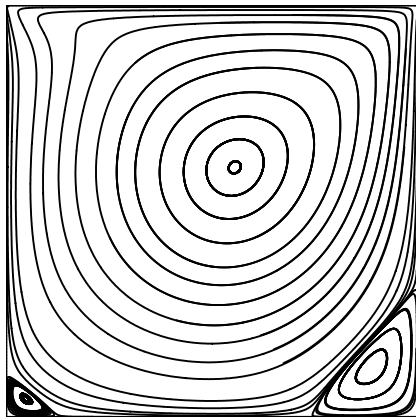


Figure 3: Streamlines of Case 2 when $Re=400$. Computational results are obtained using the present method on a 128×128 grid.

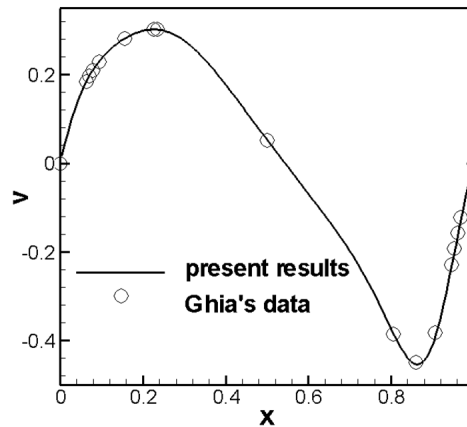


Figure 4: The v -component velocity profiles at the cavity's horizontal centerline for Case 2 when $Re=400$. Computational results are compared to Ghia's results [14] on a 128×128 grid.

second-order accuracy of the present scheme. The pressure contours are shown in Fig. 2, which exhibit no odd-even decoupling.

Case 2. Lid-driven cavity flows. The "lid-driven cavity" flows have been established as a standard "benchmark" test for numerical methods of incompressible fluid dynamics [12]. Fig. 3 depicts the stream lines of the $Re=400$ flows using the present method on the 128×128 uniform grid. The present method accurately reproduces the formation of the primary and two secondary vortices, with flow structures similar to those given in [12]. Fig. 4 presents a comparison of the velocity distributions at the horizontal centerline of the cavity that are computed using the present method and the vorticity-stream-function method [12] respectively. The agreement is excellent.

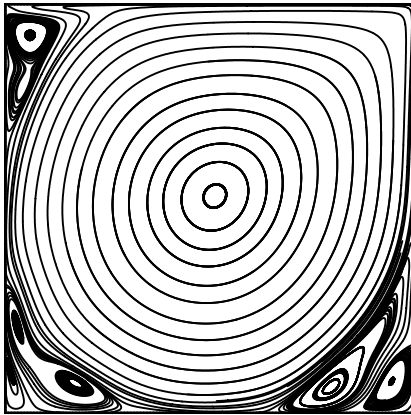


Figure 5: Streamlines of Case 2 when $Re=10000$. Computational results are obtained using the present method on a 128×128 grid.

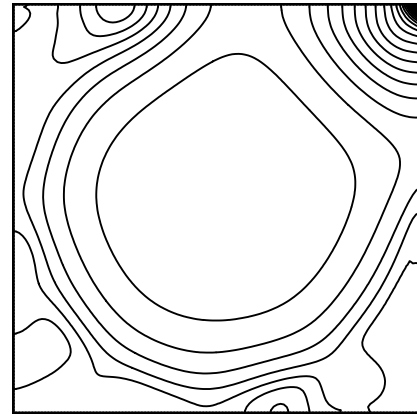


Figure 6: The pressure contours for Case 2 when $Re=10,000$. Computational results are obtained using the present method on a 128×128 grid.

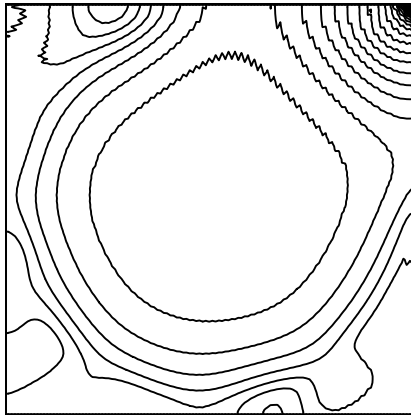


Figure 7: Same as Fig. 6, except by using the unfiltered exact projection method. The odd-even decoupling is clearly observed.

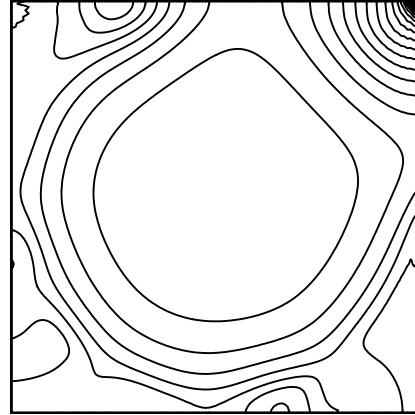


Figure 8: Same as Fig. 6, except by using the approximation projection method with the momentum interpolation method. Some minor odd-even decoupling is observed.

A high Reynolds number case with $Re=10,000$ is also computed on the 128×128 uniform grid. Unlike Ghia et al. [12] who utilized a steady-state model, our calculations show that the flow field is unsteady in this case, which was also reported in [20] where a high-order Godunov scheme was used. Fig. 5 shows the stream lines at a typical moment. The pressure contours are reported in Fig. 6. It is clear that a smooth pressure field can be predicted and no odd-even decoupling occurs. For the purpose of comparison, the pressure fields computed using the unfiltered exact projection scheme and the approximate projection scheme supplemented with the momentum interpolation technique are shown in Fig. 7 and Fig. 8 respectively. Clear checkerboard modes can be observed in Fig. 7. In this case, even the momentum interpolation technique cannot cure the odd-even decoupling.

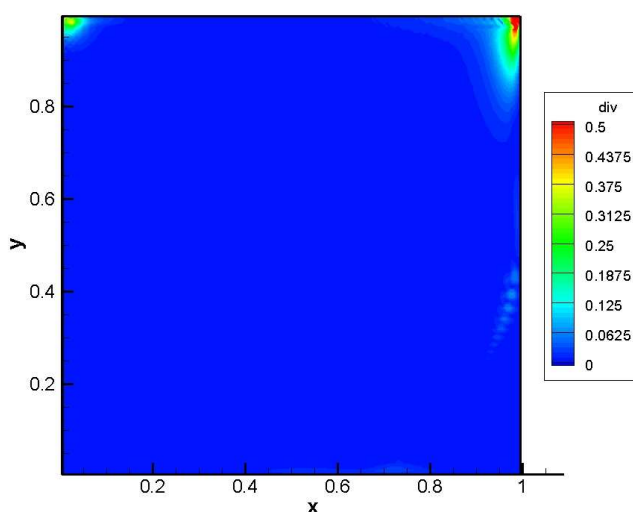


Figure 9: The discrete divergence for Case 2 when $Re=10,000$. Computational results are obtained using the approximate projection method with the momentum interpolation technique on a 128×128 grid.

pling completely and small pressure oscillations can be found near the upper-right and upper-left corners of the cavity in Fig. 8. Moreover, when the momentum interpolation technique is used, the discrete divergence $D\mathbf{u}$ is not zero, which is shown in Fig. 9. The non-divergence-free velocity field sometimes has adverse effects on the accuracy of the numerical solutions.

For a further discussion, contours of the u -component of velocity predicted by the present method for Case 2, when $Re=10,000$, is presented in Fig. 10. On the scale of Fig. 10, the contour plots obtained by using the unfiltered exact projection method and the approximate projection method combined with the momentum interpolation technique are graphically indistinguishable with Fig. 10. However, the enlarged portions of the contour plots near the upper-right corner which are displayed in Figs. 11, 12 and 13 for these three schemes respectively reveal the effects of the non-divergence-free velocity field. The discrete divergence-free projection methods predict a smooth velocity; while small "wiggles" are observed in the velocity field computed by the non-divergence-free approximate projection method.

To study the effects of grid density, the $Re=10,000$ case is recomputed on the 256×256 grid using the present method as well as the approximate projection method combined with the momentum interpolation technique. The contour plots for the pressure and the u -component of velocity near the upper-right corner of the cavity are shown in Fig. 14 and Fig. 15 respectively. For the approximate projection method, the odd-even decoupling in the pressure field becomes smaller with the increase of the grid number (and consequently the decrease of Re_G), whereas the velocity oscillations due to the non-divergence-free effect of the velocity field remain visible when compared with the numerical results of the present method.

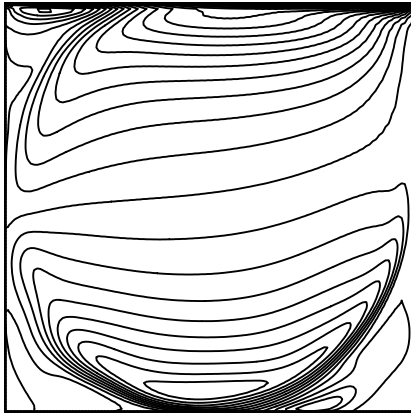


Figure 10: The u -component of velocity contours for Case 2 when $Re=10,000$. Computational results are obtained using the present method on a 128×128 grid.

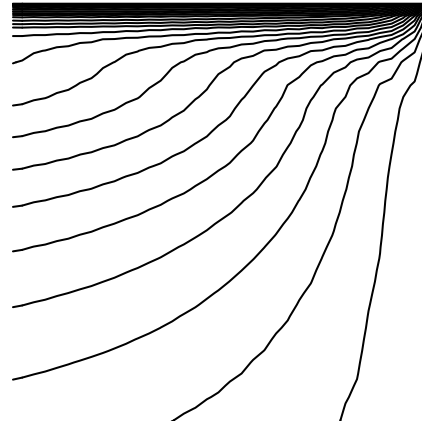


Figure 11: The u -component of velocity contours for Case 2 when $Re=10,000$. Computational results are obtained using the present method on a 128×128 grid. The enlarged view near the upper-right corner.

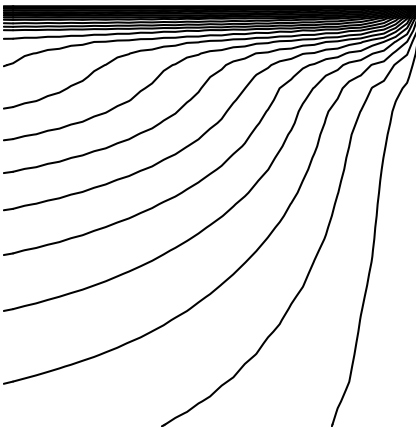


Figure 12: Same as Fig. 11, except by using the un-filtered exact projection method.

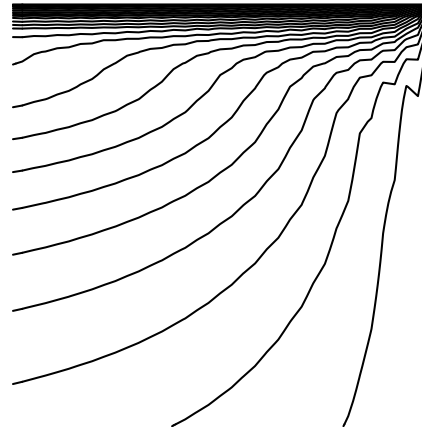


Figure 13: Same as Fig. 11, except by using the approximation projection method combined with the momentum interpolation technique. Some minor oscillation in the u -component of velocity field is observed.

6 Conclusion

In this paper, a procedure for the implementation of the second-order incremental-pressure projection scheme on collocated grids is presented. The exact discrete projection method is used to compute the velocity field, which ensures the discrete velocity divergence is zero. In order to eliminate the odd-even decoupling in the pressure field, a filtering procedure is proposed and applied to the pressure field. We have shown this filter recovers the grid scale ellipticity in the pressure field. The present projection method

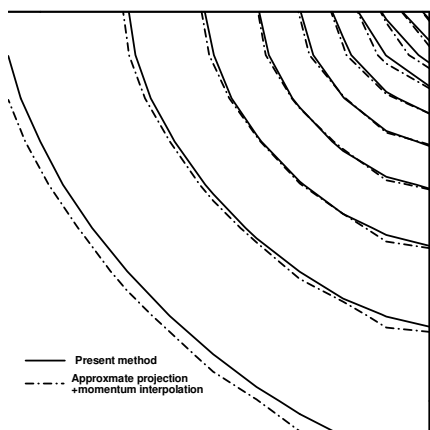


Figure 14: The pressure contours for Case 2 when $Re=10,000$. Computational results are obtained on a 256×256 grid using the present method (the solid lines) and the approximation projection method combined with the momentum interpolation technique (the dash-dotted lines).

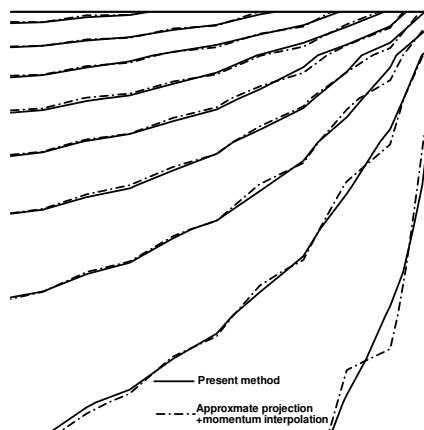


Figure 15: Same as Fig. 14, except that the contour lines of the u -component of velocity are shown.

shares some important properties of the projection method on the staggered grid, e.g., the discrete divergence is zero and the h -ellipticity measure E_h is unity. Numerical experiments indicate that the present method is second-order accurate and the odd-even decoupling in the pressure field can be removed effectively.

Acknowledgments

This work was supported by Project-10572075 of NSFC.

References

- [1] A. S. Almgren, J. B. Bell and W. G. Szymczak, A numerical method for the incompressible Navier-Stokes equations based on an approximate projection, *SIAM J. Sci. Comput.*, 17 (1996), 358-369.
- [2] S. W. Armfield, Finite difference solutions of the Navier-Stokes equations on staggered and non-staggered grids, *Comput. Fluids*, 20 (1991), 1-17.
- [3] S. W. Armfield, Ellipticity, accuracy, and convergence of the discrete Navier-Stokes equations, *J. Comput. Phys.*, 114 (1994), 176-184.
- [4] I. E. Barton, D. Markham-Smith and N. Bresslo, Finite volume scheme for the solution of fluid flow problems on unstructured non-staggered grids, *Int. J. Numer. Meth. Fluids*, 38 (2002), 747-768.
- [5] J. B. Bell, P. Colella and H. M. Glaz, A second order projection method for the incompressible Navier-Stokes equations, *J. Comput. Phys.* 85 (1989), 257-283.
- [6] O. Botella, On the solution of the Navier-stokes equations using Chebyshev projection schemes with third-order accuracy in time, *Comput. Fluids*, 26 (1997), 107-116.

- [7] D. L. Brown, R. Cortez and M. L. Minion, Accurate projection methods for the incompressible Navier-Stokes equations, *J. Comput. Phys.*, 168 (2001), 464-499.
- [8] A. J. Chorin, Numerical solution of the Navier-Stokes equations, *Math. Comput.*, 22 (1968), 745-762.
- [9] A. W. Date, A complete pressure correction algorithm for solution of incompressible Navier-Stokes equations on non-staggered grid, *Numer. Heat Tr. B-Fund.*, 29 (1996), 441-458.
- [10] E. Dormy, An accurate compact treatment of pressure for collocated variables, *J. Comput. Phys.*, 151 (1999), 676-683.
- [11] J. K. Dukowicz and A. S. Dvinsky, Approximate factorization as a high order splitting for the implicit incompressible flow equations, *J. Comput. Phys.*, 102 (1992), 336-347.
- [12] U. Ghia, K. N. Ghia and C. T. Shin, High-Re solutions for incompressible flow using the Navier-Stokes equations and a multi-grid method, *J. Comput. Phys.*, 48 (1982), 387-411.
- [13] F. H. Harlow and J. E. Welch, Numerical calculation of time dependent viscous incompressible flow of fluid with a free surface, *Phys. Fluids*, 8 (1965), 2182-2189.
- [14] J. van Kan, A second-order accurate pressure-correction scheme for viscous incompressible flow, *SIAM J. Sci. Stat. Comput.*, 7 (1986), 870-891.
- [15] J. Kim and P. Moin, Application of a fractional-step method to incompressible Navier-Stokes equations, *J. Comput. Phys.*, 59 (1985), 308-323.
- [16] M. Lai, J. B. Bell and P. Colella, A projection method for combustion in the zero Mach number limit, in: J. L. Thomas (Ed.), *Proc. AIAA 11th Computational Fluid Dynamics Conference*, AIAA Paper 93-3369, 1993, pp. 776-783.
- [17] J. G. Liu, J. Liu and R. L. Pego, On incompressible Navier-Stokes dynamics: A new approach for analysis and computation, *arXiv:math.AP/0503212*, 2005.
- [18] M. Liu, Projection methods for numerically solving the incompressible flows, PhD thesis, Tsinghua University, China, 2004.
- [19] M. Liu, Y. X. Ren and H. X. Zhang, A class of fully second order accurate projection methods for solving the incompressible Navier-Stokes equations, *J. Comput. Phys.*, 200 (2004), 325-346.
- [20] R. R. Nourgaliev, T. N. Dinh and T. G. Theofanous, Godunov-Bi-Grid-Interpolation-Based Projection Method, CRSS-Research Report 07/04-1, July 17, 2003.
- [21] C. M. Rhie and W. L. Chow, Numerical study of the turbulent flow past an airfoil with trailing edge separation, *AIAA J.*, 21 (1983), 1525-1532.
- [22] W. J. Rider, Filtering non-solenoidal modes in numerical solutions of incompressible flows, *Int. J. Numer. Meth. Fluids*, 28 (1998), 789-814.
- [23] J. Shen, J. L. Guermond and P. Mineev, An overview of projection methods for incompressible flows, *Comput. Method. Appl. Mech. Engrg.*, 195 (2006), 6011-6045.
- [24] J. C. Strikwerda, Finite difference methods for the Stokes and Navier-Stokes equations, *SIAM J. Sci. Stat. Comput.*, 5 (1984), 56-68.
- [25] R. Temam, Sur l'approximation de la solution des equations de Navier-Stokes par la methode des pas fractionnaires, *Arch. Ration. Mech. Anal.*, 32 (1969), 377-385.
- [26] H. A. van der Vorst and C. Vuik, GMRESR: A family of nested GMRES methods, *Numer. Linear Algebra Appl.*, 1 (1994), 369-386.
- [27] Y. Zang, R. L. Street and J. R. Koseff, A non-staggered grid, fractional step method for time-dependent incompressible Navier-Stokes equations in curvilinear coordinate, *J. Comput. Phys.*, 114 (1994), 18-33.